DOI:
10.1039/C6CP05714D

Document Version
Peer reviewed version

Journal Name

ARTICLE TYPE

Cite this: DOI: 10.1039/xxxxxxxxxx

Specific effects of monovalent counterions on the structural and interfacial properties of dodecyl sulfate monolayers†

Daniel T. Allen,[a] Yussif Saaka,[b], Luis Carlos Pardo,[c] M. Jayne Lawrence,[b] and Christian D. Lorenz,[a*]

Received Date
Accepted Date

DOI: 10.1039/xxxxxxxxxx

www.rsc.org/journalname

A series of molecular dynamics simulations have been conducted in order to study the specific ion effects of Li^+, Na^+, Cs^+ and NH_4^+ cations on dodecyl sulfate (DS^-) monolayers. Varying the counterion had no appreciable effect on the structure of the surfactant molecules within the different monolayers. However, the different counterions have a significant effect on the interfacial properties of the monolayer. In particular, we have investigated to what extent each of the counterions is dehydrated when interacting with the DS^- headgroup, the specific interactions between the counterions and the headgroup and the salt bridging of the headgroups caused by each counterion. The NH_4^+ ions are found to directly compete with water molecules to form hydrogen bonds with the DS^- headgroup and as a result the ammonium dodecyl sulfate monolayer is the least hydrated of any of those studied. The Cs^+ ions are strongly bound to the headgroup and weakly hydrated, such that they would prefer to displace water in the DS^- hydration shell to interact with the headgroups. In the case of the Li^+ ions, they interact almost as strongly with the DS^- headgroups as the Na^+ ions, but are generally less hydrated than the Na^+ ions and consequently the lithium dodecyl sulfate monolayers are less hydrated than the sodium dodecyl sulfate monolayers. Therefore, by changing the counterion, one can modify the interfacial properties of the surfactant monolayer, and thus affect their ability to encapsulate poorly water soluable drug molecules, which we discuss further in the manuscript.

1 Introduction

The ability of surfactant molecules to adsorb to the air/water interface is crucial in a variety of application areas including the production of pharmaceutical, food and personal care products, mineral separation processes, petroleum recovery and environmental remediation [1–8]. As a result, there has been and continues to be a wealth of scientific research using an array of experimental [9–22] and simulation [21–34] approaches in an attempt to understand the behaviour of various surfactant molecules, and the self-assembled structures which they form, at the air/water interface. The underlying chemistry of any given surfactant molecule will determine its adsorption properties, which are dependent upon the relative strengths of the hydrophobic and hydrophilic interactions that are derived from the chemical nature of the tail and headgroups of the surfactant molecule, respectively.

In this study, we have investigated dodecyl sulfate (DS^-; $C_{12}H_{25}SO_4$, as shown in Figure 1), which is one of the more common anionic surfactants utilized in the various applications listed previously, with several different monovalent counterions (Li^+, Na^+, Cs^+ and NH_4^+, as shown in Figure 1). Specifically, we are interested in understanding how the different counterions affect the interfacial properties of the monolayers that form at the air/water interface. This interest is driven by the results of recent experimental work using a combination of density, viscosity and small angle neutron scattering experiments, which showed that ammonium dodecyl sulfate (ADS) micelles solubilised fewer molecules

[a] Theory & Simulation of Condensed Matter Group, Department of Physics, Strand Campus, King's College London, Strand, London WC2R 2LS, England. E-mail: chris.lorenz@kcl.ac.uk
[b] Pharmaceutical Biophysics Group, Institute of Pharmaceutical Science, King's College London, Franklin-Wilkins Building, 150 Stamford Street, London SE1 9NH, England.
[c] Departament de Fisica i Enginyeria Nuclear, Escola TÃĺcnica Superior d'Enginyeria Industrial de Barcelona (ETSEIB), Universitat Politecnica de Catalunya, 08028 Barcelona, Catalonia, Spain.

† Electronic Supplementary Information (ESI) available: Nonbond parameters for ions and functional forms of the nonbond potential energy used in simulations; Definition of the molecular axis sets used to study the orientation of water molecules around the headgroup; Plots of the radial distribution functions of interfacial interactions; Plots of intrinsic densities of water and surfactant molecules. See DOI: 10.1039/b000000x/

of poorly water soluble testosterone derivatives than sodium dodecyl sulfate (SDS) micelles, although the ADS micelles exhibited a lower level of hydration and formed bigger micelles[35]. Therefore, seemingly this difference in the solubilisation of the drug molecules is due to the change in the interfacial properties of the self-assembled surfactant micelles caused by the various counterions. In the current study we are equating the interfacial behavior of the surfactant monolayer to that of the surfactant micelles. While the interface of a monolayer is less complex than that of a micelle, the two self-assembled structures are in thermodynamic equilibrium with one another and are found to both exist in experimental systems when the concentration of surfactants is in excess of the cmc.

Other studies have been carried out investigating the effect of varying the counterion of anionic surfactants on the ability of the micelles to solubilise molecules. Kim *et al.* found that both the aggregation number of the resulting micelles and the total solubilisation of pyrene in the DS^- aggregates increases as the counterion is changed from Li^+ to Na^+ to NH_4^+ but the number of pyrene solubilised per surfactant molecule is only slightly increased[36]. Cohen *et al.* found that the solubilisation of a corn protein, zein, decreases as the counterion used with a similar anionic surfactant, linear alkylbenzene sulfonate, is changed from Li^+ to Na^+ to K^+ to NH_4^+, with an even larger decrease observed when using the divalent cation Mg^{2+}[6].

The effect that the counterion has on the self-assembly and the structure of DS^- surfactants in aqueous systems, particularly for micellar systems[37–42] has been previously studied using both experimental and simulation methods. Molecular dynamics (MD) simulations of Li^+, Na^+ and NH_4^+ cations with DS^- micelles in aqueous solution by Rakitin and Pack[40] showed that the most compact structure for a micelle occurs with Li^+ cations that penetrate considerably deeper into the micelle than either Na^+ or NH_4^+ cations. Zana and coworkers used fluorescent measurements to determine that the aggregation number of ADS micelles is larger than those for SDS micelles and similar in size to caesium dodecyl sulfate (CDS) micelles[39,41]. Sammalkorpi *et al.* used MD simulations to show that ionic strength of the solution affects not only the aggregate size of the resulting DS^- micelles but also their structure, where specifically they found that the presence of $CaCl_2$ induces more compact and densely packed micelles than those in the presence of NaCl[42].

In an attempt to gain a clear understanding of the interfacial properties of DS^- surfactants with different counterions, experimental and simulation studies of monolayer systems have also been carried out. Neutron reflection and surface tension measurements have been used by Lu *et al.* to determine that the area per molecule of DS^- surfactant monolayers and the number of water molecules per headgroup decreases as the counterion is changed from Li^+ to Na^+ to Cs^+[9]. Using MD simulations Hantal *et al.* found that the distance between the peaks in the density of the cations and the DS^- ions depends on the size of the cation and the surface density of the anionic surfactant using MD simulations of DS^- monolayers with Li^+, Na^+, K^+, Rb^+ and Cs^+ counterions[28]. MD simulations of SDS monolayers in contact with solutions of NaCl, $MgCl_2$ and $CaCl_2$ salts have been carried out by Chen *et al.* from which they found that the sulfate groups are less bridged by ions in the divalent salts and more solvated by water and the alkyl tails become more disordered than for the monovalent salt[34]. While these studies have provided insight into the specific monolayer systems that were studied, they also reveal more detail into the general phenomena that drive the behaviour of ionic solutions at air/water interfaces which is of significant importance in the colloidal and interfacial science field, as is highlighted by several recent review articles[43–45].

Generally, ion specificity within a wide range of systems is usually referred to as Hofmeister effects, in acknowledgement of the pioneering work done by Franz Hofmeister[46,47] that systematically classified ions in sequences based on their influence on protein solubility and denaturation (these sequences are now commonly referred to as the Hofmeister series). In the *direct* Hofmeister series, Na^+ is the reference cation, with Li^+ being more kosmotropic (more hydrated) than Na^+ and Cs^+ and NH_4^+ are more chaotropic (less hydrated than Na^+), such that they are ordered like $NH_4^+ < Cs^+ < Na^+ < Li^+$[43,44,48]. This order will be used as a reference while discussing our findings throughout this manuscript.

In this manuscript, we report the results of a series of MD simulations that have been used to determine the specific ion effects of lithium (Li^+), sodium (Na^+), caesium (Cs^+), and ammonium (NH_4^+) counterions with DS^- monolayers. Notably, we have found that the ability for NH_4^+ cations to form hydrogen bonds directly with the DS^- headgroup leads to a significant dehydration of the headgroups as compared to what is observed with the other monatomic monovalent ions studied. As a result, we observe significant changes in the interfacial properties of the surfactants and the interfacial water in the ADS monolayer systems as compared to that observed in the other monolayers. To the best of our knowledge this study represents the first detailed investigation of the interactions between these monovalent ions and DS^- monolayers.

The details of the systems that we have simulated and of the simulation protocol that has been applied in this study is presented in Section 2 of this manuscript. The various measurements that we have used to characterise the interfacial properties reported in this manuscript are described in Section 3. Section 4 reports the structural properties of the DS^- monolayers and the interactions between the DS^- headgroup and the water molecules and counterions. Finally, in Section 5, we discuss our results in light of the measurements that have been previously reported from both experimental and simulation studies and we discuss how these measured properties may lead to the observed difference in solubilisation of testosterone derivatives within SDS and ADS micelles.

2 Simulation Details

Results are reported from four all-atom molecular dynamics (MD) simulations which were used to investigate the structural and interfacial properties of dodecyl sulfate (DS^-) surfactant monolayers at the air/water interface with different counterions (Li^+, Na^+, Cs^+, NH_4^+) present. The monolayer systems are all comprised of two monolayer leaflets separated by a 60 Å thick water

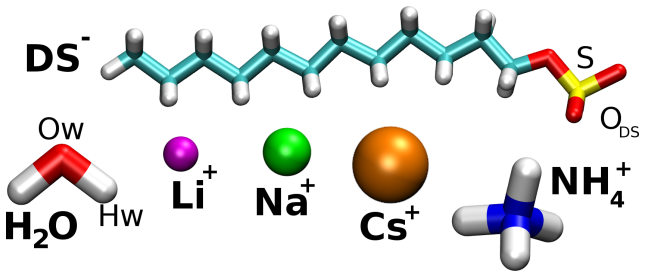

Fig. 1 The chemical structures of the molecular species featured in the current study: DS^-, water and counterions. The colours cyan, grey, red, yellow and blue are used to represent the elements: carbon, hydrogen, oxygen, sulphur and nitrogen respectively for the non-monatomic species. The monatomic counterions Li^+, Na^+ and Cs^+ are depicted in the colours magenta, green and orange respectively.

slab. Each leaflet contains 100 DS^- monomers within a simulation box with $x-$ and $y-$ dimensions of 69.28 Å each such that the area per surfactant is ~ 48 Å^2. This is in agreement with the experimentally determined value for SDS monolayers[49] and is used for all reported monolayers so that the system properties can be fairly compared whilst being modeled at a realistic value of area per surfactant. Periodic boundary conditions were applied in all dimensions, with the $z-$ dimension of the simulation box set to 200 Å to ensure that the monolayers do not interact with one another through the periodic boundary in the $z-$axis. The centre of masses of each of the systems were constrained to be at the position $z = 0$ throughout the simulations in order to make the analysis of the simulations as easy as possible.

The initial structures of the SDS and ADS monolayers were built using the Packmol software package[50] and were neutralized by the addition of 100 Na^+/NH_4^+ counterions per leaflet, placed near the headgroup regions of the DS^- molecules. For both of these systems, 9600 water molecules were subsequently placed within the simulation box between the monolayers to form 60 Å water slabs with a resulting water density of 1 g/ml. Energy minimizations were performed on both systems using 100000 steps as the maximum number of force/energy evaluations and the minimized states of these systems were then simulated in the constant NVT ensemble for 10 ns for thermalization. Finally, 50 ns production runs were performed in the NVT ensemble from which the analysis is conducted. For lithium dodecyl sulfate (LDS) and CDS, the final state of the SDS monolayer simulation was taken as a starting point and the parameters for the point-like counterions were simply modified to represent the appropriate ionic species. The above simulation protocol was repeated for the LDS and CDS monolayers.

All monolayer simulations were performed at T = 300 K using the LAMMPS simulation package[51] with the CHARMM force field[52,53] for the description of both inter- and intra-molecular interactions of the DS^- and the various counterions[54,55]. The nonbond parameters for the ions and the functional forms used to describe the nonbond interactions in our simulations are included in the Supplementary Information. The TIP3P water model[56], which was modified for the CHARMM forcefield[57], was used to describe interactions involving water. This combination of forcefields has previously been shown to give a good description of SDS micelles[58,59].

The van der Waals interactions were cut-off at 10 Å whilst the electrostatic interactions were cut-off at 12 Å. The PPPM method[60] was used to compute long-range Coulombic interactions. The equilibration and production runs for all monolayer simulations utilized the Nose-Hoover thermostat[61] to fix the system temperature. A timestep of 2 fs was used in all simulations to ensure stable integration of Newton's equations of motion with the *velocity Verlet* algorithm whilst all hydrogen-containing bonds were constrained using the SHAKE algorithm[62]. The measurements discussed in the following sections were conducted using the last 10 ns of the production periods obtained, in which the dynamics were deemed to be stable for each simulation.

3 Analysis of simulation trajectories

3.1 Intrinsic surfaces

The ability to locate the monolayer/water interface is of great importance as we are particularly interested in the effect that the various counterions have on the structure of this interface. To study properties with reference to the interface, the concept of the *intrinsic surface* is introduced. The intrinsic surface of the monolayer is denoted by $\xi(\mathbf{R}) = \xi(x,y)$. We require a continuous surface to represent the location of the DS^-/water interface for any given (x,y), constructed from a finite number of anchor points. In this particular case, the choice of anchor points is trivial: the sulphur atoms in the DS^- headgroups.

There are a number of different ways of constructing the intrinsic surface for surfactant/water interfaces reported in the literature. These include the *intrinsic sampling method* proposed by Tarazona *et al*[63] which has been applied to a study of surfactant monolayers at water-oil and water-vapour interfaces by Bresme *et al*[64]. Chandler *et al* utilized a coarse-grained density field approach to establish the interface between water and heterogeneous surfaces[65]. For computational efficiency, the current study employs the algorithm proposed by Berkowitz *et al*[66]. In essence, this method is performed by projecting the location of a particle of interest and the anchor points used to define the interface on to the *x-y* plane. Next, the closest anchor point to the particle of interest within this projected two-dimensional representation is established and then the position of the intrinsic surface for the particle of interest is assigned the value of the z-coordinate of the closest anchor point.

The intrinsic density of a given atomic species is defined mathematically as:

$$\widetilde{\rho}(z) = \left\langle \frac{1}{A_0} \sum_{i=1}^{N} \delta(z - z_i + \xi(\mathbf{R_i})) \right\rangle \qquad (1)$$

where the summation indexed by i runs over all N particles of a given atomic species, $\xi(\mathbf{R_i})$ represents the *intrinsic surface* for a given configuration, $\mathbf{R_i} = (x_i, y_i)$ is the location of particle i in the *x-y* plane for a given configuration, A_0 is the cross sectional area of the interface, z denotes the vertical distance from the DS^-/water interface to particle i where values of $z > 0$ and $z < 0$ represent locations within the water slab and towards the vacuum region

respectively. Finally z_i is the z-coordinate of the i^{th} particle.

3.2 Measurement of monolayer structural properties

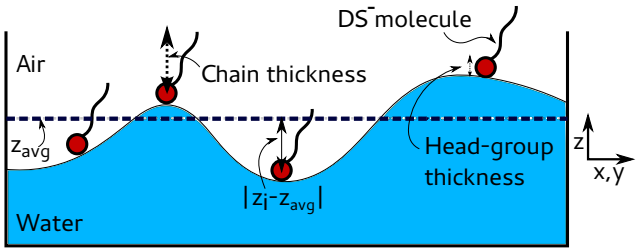

Fig. 2 Schematic diagram of the measured structural properties of DS^- monolayers. The thick dashed line represents the average z-coordinate of the DS^- headgroups in a monolayer, from which $|z_i - z_{avg}|$ is calculated and used to quantify monolayer roughness. Chain thickness and headgroup thickness measurements are also shown.

We have measured various structural properties of the DS^- monolayers in order to quantify how these are affected by the different counterions. In the following paragraphs, we summarise how the reported quantities were calculated, and Figure 2 shows a pictoral description of each of these calculations as well.

The instantaneous *monolayer thickness* is calculated by taking the end to end vectors of the surfactant molecules within a monolayer and projecting these on to the z-axis and then taking the average. Ensemble-averaged monolayer thickness values were calculated by averaging the instantaneous monolayer thickness values.

Meanwhile, the instantaneous *thickness of the headgroup region* of the DS^- monolayer is calculated in a similar manner as the full monolayer thickness. The thickness of a headgroup in a given DS^- molecule is determined by first establishing the maximum and minimum z-coordinates of the four oxygen atoms in the headgroup, and then taking the difference between the maximum and minimum of these z-values. Then to find the thickness of the headgroup region of a monolayer, we average over all DS^- molecules.

To quantify the *monolayer interfacial roughness*, the root-mean-squared (RMS) deviation value of the difference between the $z-$coordinate of a S atom in the DS^- headgroup and the mean value of the $z-$coordinates of all the S atoms present in a monolayer within a given configuration of the trajectory was calculated: $|z_i - z_{avg}|$, as shown in Figure 2.

3.3 Radial distribution functions and spatial density maps

In this manuscript, we report the results of radial distribution functions (rdfs) and spatial density maps (SDMs) in order to describe the interactions between the DS^- headgroups and the ionic solutions in the various systems. In doing so, molecular axes are decided upon and assigned to all molecules in the system by the addition of pseudoatoms which form an orthogonal basis set, as shown in the SI. It is known that DS^- forms hydrogen bonds with water molecules via the ionic oxygen atoms in the headgroup. The simulation parameters are identical for these ionic oxygen atoms and thus it is reasonable to assume that the interaction between any one of them and the surrounding water molecules is the same. For this reason, the molecular axis for the surfactant molecule is chosen such that the z-axis points along the vector connecting the sulfur atom to one of the ionic oxygen atoms. In this way, we can study the behavior of water around just one of the ionic oxygen atoms in a very detailed manner. Similarly, for water/ammonium molecules the z-axis points from the oxygen/nitrogen atom to the hydrogen atom which is involved in the hydrogen bond. Of the four different counterions studied, ammonium is the only species which has an orientation as it is not point-like.

The position of a molecule is given by the pseudoatom, which forms the origin of the axis set on that molecule. The position and orientation of any two molecules in the system is described completely by the vector: $(r, \cos\theta_{cm}, \phi_{cm}, \theta_{or}, \phi_{or}, \psi_{or})$, where r denotes the magnitude of the separation between the two molecular axis sets, θ_{cm} and ϕ_{cm} denote the azimuthal angle and polar angle of the neighbouring molecule around the axis of the central molecule, respectively, and θ_{or}, ϕ_{or} and ψ_{or} are the three principal Euler angles of the neighbour molecule relative to the axis of the central molecule. Thus both the position and the orientation of a neighbouring molecule relative to the fixed axis set of a central molecule is completely described by these 6 variables.

Radial distribution functions are used to identify the nearest neighbour distance, which is defined as the distance corresponding to the first minimum in the rdf curves. SDMs of different neighbouring atomic species are produced by plotting points at the observed positions of the neighbouring atoms relative to the central molecule axes $(r, \cos\theta_{cm}, \phi_{cm})$ throughout the last 10 ns of the production period. An isosurface is constructed based upon the density of these points in space. The resulting isosurface represents the most probable spatial region(s) to find a particular nearest neighbour atom and is advantageous over rdf curves as it contains information about three spatial dimensions as opposed to just one. In this way, an intuitive representation of positions of nearest neighbours is constructed around the central molecule. Note that in the remainder of the manuscript, the terms 'SDM' and 'cloud' will be used interchangeably.

Bivariate probability plots can be constructed in conjunction with SDMs. These show the probability of finding a nearest neighbour at a given set of azimuthal and polar angles $(\cos\theta_{cm}, \phi_{cm})$. These have a direct correspondence with the appropriate SDMs however they reveal the varying probability of neighbours *within* the isosurfaces. If one takes only the data from the maximum region of these bi-variate probability plots then the orientational states of neighbour molecules in a highly localized region of space can be studied by examining the Euler angles adopted by these molecules.

The orientational state of a neighbour molecule relative to the fixed axis of a central molecule can be represented in a 3-dimensional space, where each individual point corresponds to a unique orientation of the neighbour molecule. The three axes, x, y and z in this space represent the three principal Euler angles. In a similar manner to the SDMs, points are plotted which represent observations of orientations adopted by nearest neighbour molecules within the selected localized region in space. An iso-

surface can be constructed which forms a trivariate plot. These trivariate plots can then be used to elucidate the most probable orientational states adopted by the neighbour molecule. This is achieved by cutting the trivariate plot at periodic intervals along the axis which has the largest variance. Each slice is a bivariate probability distribution of two of the Euler angles, given a third (determined by where the slice was taken). From each slice, the most probable orientation is determined by the maximum of the resulting 2d histogram.

4 Results

In this section, we present our findings from four different surfactant monolayer simulations each composed of different counterions, namely LDS, SDS, CDS and ADS. We have investigated the effect that the different monovalent counterions have on the structure of the surfactant monolayers, the hydration of the DS^- headgroups, the structure of the water around the headgroup and the binding of the ions with the headgroups. The radial distribution functions, spatial density maps and bivariate probability plots reported in this study were constructed by utilizing the ANGULA software package which is available for free download (https://gcm.upc.edu/en/members/luis-carlos/angula/ANGULA).

4.1 Intrinsic density profiles

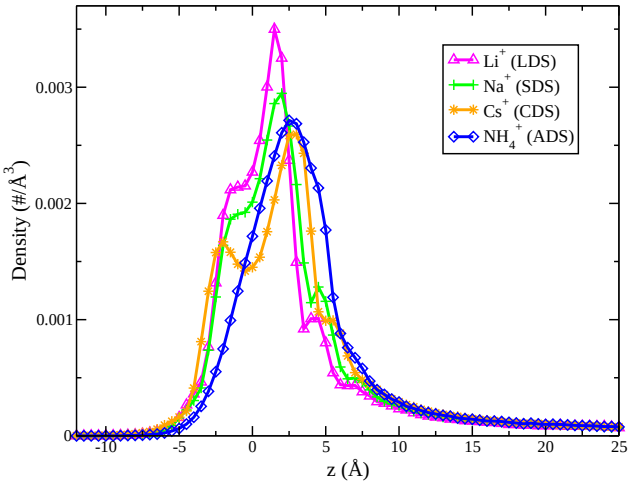

Fig. 3 Intrinsic density profiles of the Li^+ (magenta), Na^+ (green), Cs^+ (orange) and NH_4^+ (blue) ions.

Intrinsic density profiles are used to study the location of counterions in the simulations with respect to the monolayer interface, see Figure 3. On these plots, positive and negative values of z correspond to positions towards the bulk water and towards the hydrocarbon tail regions, respectively. These plots reveal large peaks in the ion density at small positive values of z, corresponding to the most probable location of the counterions at the surfactant/water interface on the side of the bulk water. The density peaks all tend to zero as we move into the bulk water i.e, positive values of z and the counterion intrinsic density curves are coincident at large values of z which suggests that the counterions' behaviour differs around the interface, not in the bulk water.

The Li^+ and Na^+ intrinsic density profiles exhibit 'shelves' on both sides of the main interfacial density peak. These arise from ions being located in the vicinity of the surfactant/water interface. The value of the cation density within the LDS monolayer is larger than that within the SDS monolayer (values of $z \leq 0$), conversely for the 'shelf' on the other side of the main peak, the Na^+ peak is at a larger density than the Li^+. This is most likely due to the size difference between these ionic species: lithium is smaller and thus more able than sodium to fit into the small spaces in between the sulfate headgroups of the DS^- molecules.

Cs^+ ions are the largest of the point-like ions in the current study and their density follows the same trend of decreasing density within the monolayer with increasing ion size. Cs^+ ions are large in comparison to Li^+ and Na^+ and their intrinsic density profile exhibits a minima and a secondary peak of density within the monolayer rather than a shelf. This minima corresponds to the region just under the surfactant headgroups and is located at $z = -0.5$ Å. This minima arises due to the larger size of Cs^+ and the many steric interactions resulting from the surfactant headgroup oxygen atoms in this location. Because of these strong interactions, Cs^+ will likely be forced either within the monolayer or to larger z values. Cs^+ exhibits a shelf at $z \sim 5$ Å, a feature which is also present in the intrinsic density profiles for Li^+ and Na^+.

The intrinsic density profile of the nitrogen atoms in the ammonium ions is also plotted. Only the nitrogen atom density was calculated so that the total number of atoms used to construct the intrinsic density plots was equal and thus the integral under all of the curves are equal. This ensures that meaningful comparisons of density can be drawn between the different ionic species. The nitrogen atoms in the NH_4^+ ions exhibit the broadest peak of the different counterion species. The position of this peak is at a larger value of z than the peaks for the Li^+ and Na^+ ions.

For the monatomic ions, there is a trend of decreasing density inside the monolayer as the ionic radii increases. The density of NH_4^+ ions within the monolayer is lower than any of the monovalent cations. This trend agrees with what is explained in a recent publication by Sivan in which an unified explanation of various interfacial interactions of ions including the phenomena that result in small cations being attracted to hydrophilic interfaces[45].

Additionally, when investigating the intrinsic density of the oxygens in the headgroup and the water near the interface of the monolayers (as shown in the SI), we also see a difference between the systems with monatomic ions and the system with NH_4^+ ions. Specifically, in the systems with Li^+, Na^+ and Cs^+, we observe a distinctive interfacial peak in the intrinsic density of the oxygen atoms in the water molecules occurring at a distance of ~ 3 Å from the intrinsic surface. Also, we observe a broad distribution of the intrinsic density of the O_{DS} atoms in the surfactant headgroup which is consistently increasing throughout a range of distances from ~ -2 Å to ~ 0.5 Å from the intrinsic surfaces, with a peak at $z \sim 0.5$ Å. However, in the system with NH_4^+ cations, there is no interfacial peak in the intrinsic density of the oxygen atoms in the water molecules, which suggests that the water molecules do not pack as well into the same region of space and

are therefore less ordered than at the interfaces with the monovalent cations. Additionally, we observe two peaks in the intrinsic density of the O_{DS} atoms of the headgroup, a large peak occurring ~ 2 Å from the intrinsic surface and a smaller peak at ~ -1 Å from the intrinsic surface. Therefore, the orientation of the headgroups seems to be more constrained when they are interacting with the NH_4^+ counterions than when interacting with the other monatomic counterions.

These plots reveal that the counterions exhibit distinctly different behaviour at the monolayer interface which could have a significant effect on other monolayer structural and interfacial properties such as roughness, interfacial tension and the overall hydration of the monolayers, which will be discussed in the following sections.

4.2 Monolayer structure

The results from the calculations of the monolayer and headgroup thickness for the various systems are presented in Table 1 with the standard deviations of the measurements reported as the errors. These results reveal that the monolayer thickness is unchanged by varying the counterion, a result which is unsurprising as the counterions have little effect on the surfactant chain tilt angle (as shown in the SI), which plays a large role in determining monolayer thickness. The headgroup thickness is also unchanged when the DS^- monolayers are interacting with solutions containing different counterions. These results are consistent with those from recent neutron reflectivity measurements of LDS, SDS and CDS monolayers[9].

Whilst the monolayer and headgroup thicknesses are unchanged with counterion species, these measurements contain no information regarding roughness of the surfactant-water interface: a property which could be pivotal in determining local water structure and thus the ability of an aggregate to effectively operate as a solubilizing agent. The roughness of the LDS and ADS monolayers are the same with RMS deviation values of (2.5 ± 0.2) Å. The fluctuations of surfactants in the SDS monolayers reveal slightly larger values with an RMS of (2.7 ± 0.2) Å. The CDS monolayers however are significantly more rough with a RMS value of (3.4 ± 0.4) Å. This may be due to stacking of adjacent surfactant headgroups due to the large size of the caesium ions. See Table 1 for a summary of all of the structural properties of the various monolayers.

4.3 Dehydration of cations

We wanted to gain a better understanding to what degree the ions are dehydrated as they interact with the DS^- headgroups. Therefore, we have calculated the hydration of the counterions themselves as a function of distance from the intrinsic surface of the monolayers. The nearest neighbour distances found from the $g(r)$'s for the interaction between each cation and the O_W atoms in the water molecules were used as the metric to determine whether a given water molecule was hydrating an ion or not. The average number of hydration water molecules around a given ion was determined by averaging the number of water molecules that are within the nearest neighbor distance from the g(r), taking precautions not to double count any water molecules around a single ion.

Figure 4 shows the mean hydration number of the different counterion species as a function of their distance to the interface, z. For all different counterions we see that the hydration number is always at a maximum in the bulk water as one might expect. The hydration numbers of the various ions in the bulk water region (large values of z) are in good agreement with those measured using various simulation methods elsewhere: Li^+ (4.2 ± 0.4)[67], Na^+ (5.8 ± 0.4)[68], Cs^+ (9.6 ± 1.3)[69] & NH_4^+ (4.9 ± 1.4)[70].

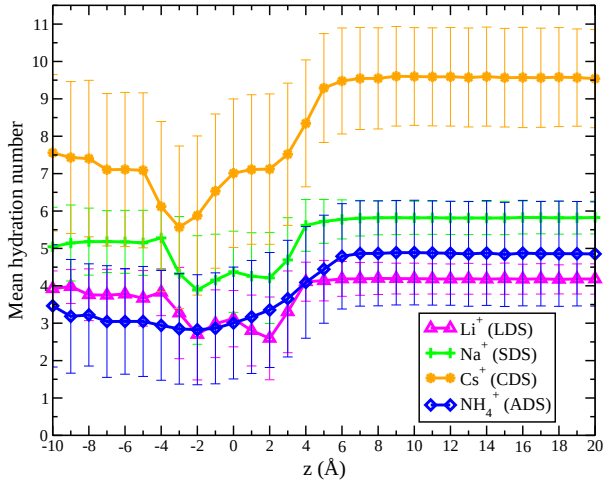

Fig. 4 The mean hydration number of the different counterions as a function of distance away from the monolayer interface, z.

For the point-like ions, at all values of z, the average number of hydrating water molecules increases with the ionic radii of the ion. We found that the most dehydrated are the Cs^+ and NH_4^+ ions as they both lose $\sim 40\%$ of their hydration shell when interacting with headgroup. Meanwhile, the Na^+ and Li^+ ions only lose $\sim 30\%$ of the water molecules within their hydration shell. This trend in the dehydration of the ions agrees well with the Hofmeister series, which states that the Cs^+ and NH_4^+ ions are the most weakly hydrated of the four we have simulated and therefore the easiest to dehydrate, while Na^+ and Li^+ are more strongly hydrated.

All systems exhibit a decrease in the mean hydration number around the cations as they approach the monolayer/water interface ($z \sim 5-6$ Å). In this region, the DS^- headgroups will start to compete with neighbouring water molecules for the interaction with the cations and therefore result in a decrease in the average number of hydrating waters within the first hydration shell of the cations.

Beyond the interface, into the hydrocarbon tails ($z < -2$ Å), the mean hydration number increases and converges at a value which is less than that in the bulk for the monatomic counterions. This increase is due to the fact that there are less atoms (O_{DS}) in this region that will compete with the water molecules for interactions with the ions and so they interact more with the ubiquitous water molecules.

Table 1 Summary of the structural properties for the LDS, SDS, CDS and ADS monolayers.

	LDS	SDS	CDS	ADS
Full Thickness (Å)	10.7 ± 0.2	10.7 ± 0.2	10.7 ± 0.2	10.7 ± 0.2
Head Thickness (Å)	2.2 ± 0.01	2.2 ± 0.01	2.2 ± 0.01	2.2 ± 0.01
Roughness (RMSD) (Å)	2.5 ± 0.2	2.7 ± 0.2	3.4 ± 0.4	2.5 ± 0.2
Hydration water #	7.3 ± 3.3	8.3 ± 3.6	7.3 ± 3.0	6.6 ± 2.8
% ions bound to headgroup	53%	55%	68%	70%

In the case of the NH_4^+ ions, we observe a dehydration of the cations starting at $z \sim 6$ Å. The decrease in hydration is then more or less monotonic until $z \sim -2$ Å, at which point the average number of hydrating water molecules plateaus. This would suggest that in general in this region, the NH_4^+ ions are interacting in a similar way with the DS^- headgroups and surrounding water molecules, and as we have seen in the intrinsic density plots that there is a continually decreasing number of ions in this region, it seems that the motion of these ions is restricted by their desire to form hydrogen bonds with the O_{DS} atoms in the surfactant headgroups.

4.4 Hydration of DS^- headgroups

Radial distribution functions have been calculated to quantify the interactions between the DS^- headgroup and the water molecules. Figures in the SI show the rdf, $g(r)$, curves for interactions between the ionic oxygen atoms in the surfactant headgroups O_{DS} and the oxygen atoms in the water molecules O_W and the O_{DS} atoms and the hydrogen atoms in the water molecules H_W. The nearest neighbour distances, coordination numbers and $g(r)$ plots for all systems are shown in the SI.

The O_{DS}–H_W $g(r)$ shows very little change as the counterion is changed. However, the $g(r)$'s for O_{DS}–O_W show slight differences in both peak amplitude and the curve shape. These differences arise from the effect that the different cations have on the structure of the interfacial water molecules, which will be discussed in greater detail in the following sections.

Using the nearest neighbour distances between sulfur atoms in the DS^- headgroup, S_{DS}, and the O_W atoms for each system ($d_{S,O_W} = 4.95$ Å), the number of hydration water molecules around a surfactant headgroup was determined by counting the number of nearest neighbour water molecules. Precautions were taken not to double count any water molecules around the headgroups, such that any given water molecule was only counted as hydrating one surfactant molecule at any instance in time. The values reported in Table 1 are determined by averaging over every surfactant molecule and over every configuration in the production trajectory. We found that mean values of the number of hydration waters per headgroup are ordered as follows: NH_4^+ (6.6) < Li^+, Cs^+ (7.3) < Na^+ (8.3). A similar trend has been reported in a previous simulation study of LDS, ADS and SDS micelles in solution[40].

Histograms were constructed using all snapshots from the production simulations for the different systems and are shown in Figure 5. All of these histograms show broad distributions with hydration numbers per surfactant molecule ranging from 0 to 22 (in the case of SDS). ADS has the smallest value for the average number of hydrating water molecules and also the smallest spread of values in the histogram. CDS has the same average hydration number as LDS with a slightly smaller standard deviation.

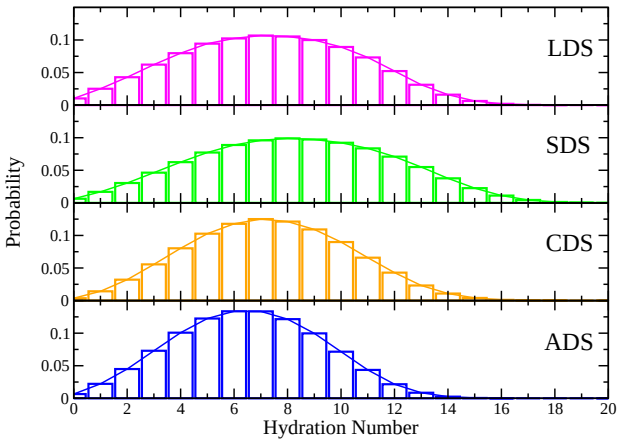

Fig. 5 Histograms showing the probability of a surfactant headgroup having a given hydration number in the monolayer simulations. The mean and standard deviation for each system is as follows: LDS – 7.3 ± 3.3, SDS – 8.3 ± 3.6, CDS – 7.3 ± 3.0 and ADS – 6.6 ± 2.8.

4.5 Interfacial water orientation

Using the methods described in Section 3.3, we were able to study the orientational states of water molecules located within a small region of the O_W SDM, which corresponds to the most probable location to find a water molecule hydrogen bonded to a DS^- headgroup.

The least probable water orientation at this particular point in space, as shown in Fig. 6a, shows the water molecule is oriented such that one H_W atom is forming a hydrogen bond with a O_{DS} atom and the other is oriented such that it points away from the air/water interface and into the bulk water region. On the other hand, the most probable water orientation at this point in space, Fig. 6b, is one in which the water molecule is oriented with one H_W atom is forming a hydrogen bond with a DS^- headgroup and the other H_W atom is directed toward the air/water interface such that it maximizes hydrogen bonding between water and surfactant headgroups. This most probable water configuration is in agreement with the configuration of the water observed in recent sum-frequency generation spectrum studies of SDS monolayers[20,22].

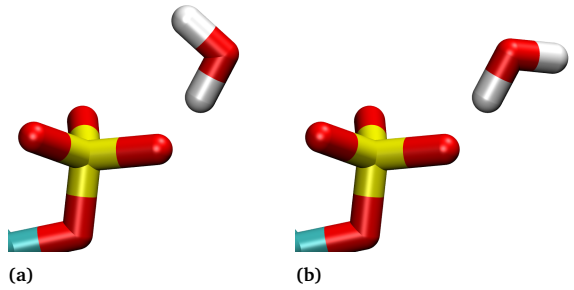

Fig. 6 Representative snapshots of the least (a) and most probable (b) orientations of a bound water molecule within a small region of space around the DS^- headgroup from the CDS simulation.

4.6 Counterion – DS^- headgroup interactions

The SI shows $g(r)$'s for the O_{DS} atoms and the counterions in the various systems. The nearest neighbour distances for each O_{DS} – counterion interaction are also summarized in the SI. From these values and the $g(r)$'s, we observe that both the separations between ions in direct contact with the sulfate headgroups (first peaks) and the separations between hydrated ions and the sulfate headgroups (second peaks) both increase in the series $Li^+ < Na^+ < NH_4^+ < Cs^+$, which is consistent with the trend of their respective ionic radii. Also, this is consistent with a previous simulation study of similar counterions with DS^- micelles[40].

While rdfs provide a one dimensional description of the interaction between two atomic species, they do not reveal where they are likely to be located in three dimensional space relative to one another. Spatial density maps (SDMs) do exactly this by providing a visual representation of the most probable spatial regions to find a neighbouring atomic species. In our study, these plots allow a three-dimensional intuitive depiction of the structure of the water molecules and counterions around the surfactant headgroups which will allow us to understand how the various ions affect the hydration shell of the DS^- headgroup.

SDMs of water molecules and counterions were produced for all of the monolayer systems and are shown for LDS, SDS, CDS and ADS in Figures 7a, 7b, 7c and 7d respectively. The SDMs produced for all of the monolayer systems reveal that the oxygen and hydrogen atoms in nearest neighbour water molecules occupy a region of space which is donut-shaped. The region representing the H_W atoms is nearer the O_{DS} than the region representing the O_W atoms, which is consistent with what we observed from the $g(r)$'s for these systems. Additionally, the diameter of the donut-shaped region for H_W atoms is smaller than that for the O_W atoms. Combining these two observations indicates that the water molecules in the first hydration shell are hydrogen bonded to the O_{DS} atoms in the headgroup, and this provides an explanation for the two donut-shaped clouds when taking into account that the $OH_{water}\cdots O_{DS}$ angle would need to be no larger than 30°.

The SDMs also reveal that the point-like counterions (Li^+, Na^+, Cs^+) have a strong preference to reside behind the nearest neighbour O_W atoms in the nearest neighbour water molecules. The Li^+ and Na^+ SDMs exhibit a very localised interaction with the DS^- headgroups, in which they both occupy circular-shaped regions behind the O_W SDMs. The SDM for Cs^+ differs somewhat from those of Li^+ and Na^+, as it exhibits larger clouds which suggest that the position of Cs^+ is less localized in relation to the surfactant headgroup. We see then that the point-like counterion clouds are located elsewhere in space from the clouds representing water molecules. From this we deduce that none of the monatomic counterions (Na^+, Li^+ and Cs^+) are likely to displace a water molecule which is hydrogen bonded to the DS^- headgroup.

Meanwhile, the NH_4^+ ions show very different behavior to the point-like ions. The SDMs for nitrogen and hydrogen atoms in NH_4^+ ions around the O_{DS} atoms are coincident with the SDMs for O_W and H_W atoms respectively, as can be seen by the blue and pink SMD in Figure 7d. This suggests that the NH_4^+ ions are able to displace interfacial water molecules from the DS^- headgroups which explains why the mean hydration water number of the ADS surfactant headgroups are significantly less than for the other systems. The NH_4^+ ions are directly competing with the water molecules for hydrogen bonding partners within the DS^- headgroups, and are therefore forming stronger interactions with the headgroup than the other monatomic cations.

The SDMs show an isosurface of the most probable regions in space to find different atomic species depicted in Fig. 7, however the probability within these SDMs varies with some regions within the clouds being more probable than others. To elucidate the variance in probability within different regions of the SDMs, bivariate plots are exploited which show the probability as a function of the polar angles $\cos\theta_{cm}$ and ϕ_{cm}. The bivariate plots for the water molecules which are hydrogen bonded to the DS^- headgroups are similar for all systems. The donut-shaped SDMs of the O_W and H_W atoms in the water molecules materialize as donut-shaped rings on the bivariate plots, as shown in Fig. 8a. These rings show a little variance in probability. There is a region of lower probability within the distribution of O_W atoms, centered at approximately $\cos\theta_{cm} = 0.3$, $\phi_{cm} = 100°$, which corresponds to a region of space between the DS^- headgroups and the hydrocarbon tails of the surfactant molecules. Within this same region, one finds the most probable location of the nitrogen atoms in the NH_4^+ ions, indicated by the sharp red region in Fig. 8b.

4.7 Salt bridging of DS^- headgroups

In order to quantify the number of counterions around a surfactant headgroup, we measured the $g(r)$ between S_{DS} and counterions and then obtained the nearest neighbour distance in the same way as for the water molecules. In contrast to the hydration water calculations, we are indeed interested in ions which are simultaneously interacting with multiple surfactants. This is an effect referred to as 'salt-bridging' in the literature.

We have determined the percentage of ions bound to the headgroup of the surfactant molecules p_{bound}, which can be used to find the degree of ionisation α by just calculating $1 - (p_{\text{bound}}/100\%)$. The values of α we find for our various systems are 0.3 (ADS), 0.32 (CDS), 0.45 (SDS) and 0.47 (LDS), which agree very well with those determined from electrical conductiv-

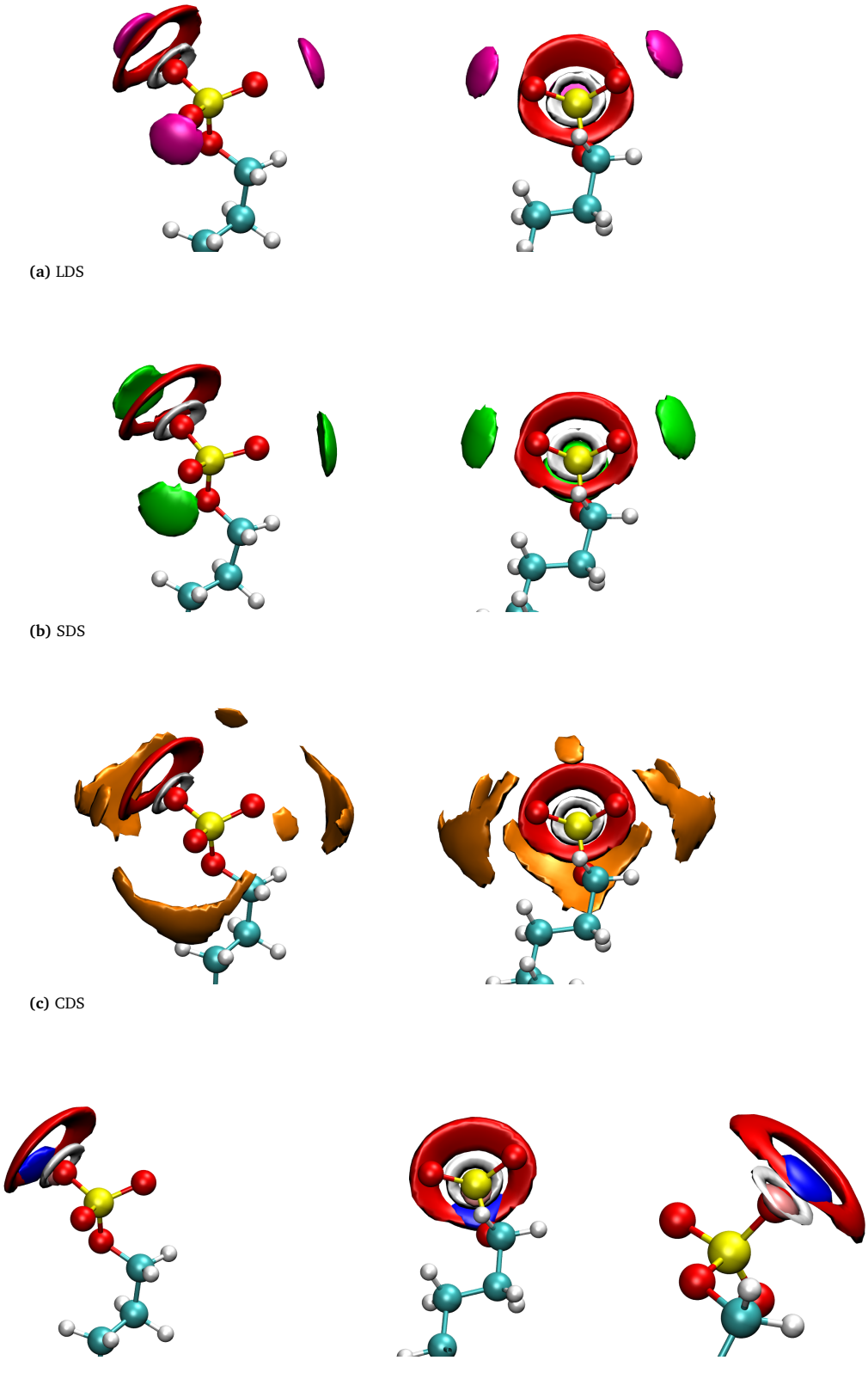

(a) LDS

(b) SDS

(c) CDS

(d) ADS

Fig. 7 Spatial density maps of the DS^- headgroups with the O_W (red clouds), H_W (grey clouds) and the (a) Li^+ ions (magenta clouds), (b) Na^+ ions (green clouds), (c) Cs^+ ions (orange clouds) and (d) the N (blue clouds) and H (pink clouds) atoms in the NH_4^+ ions.

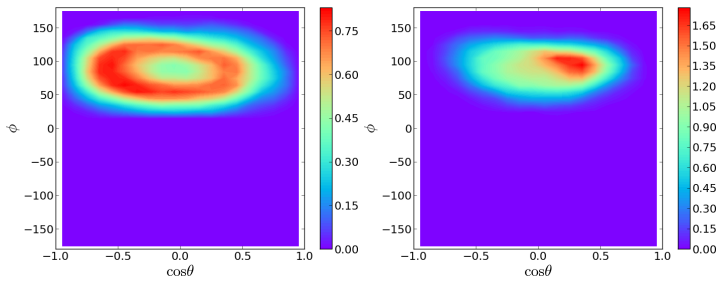

(a) Ow **(b)** N (NH_4^+)

Fig. 8 Bivariate probability density distributions of oxygen atoms in water molecules (a), and nitrogen atoms in ammonium ions (b) around the DS^- molecular axis. The contour scale bars in both plots represent probability density.

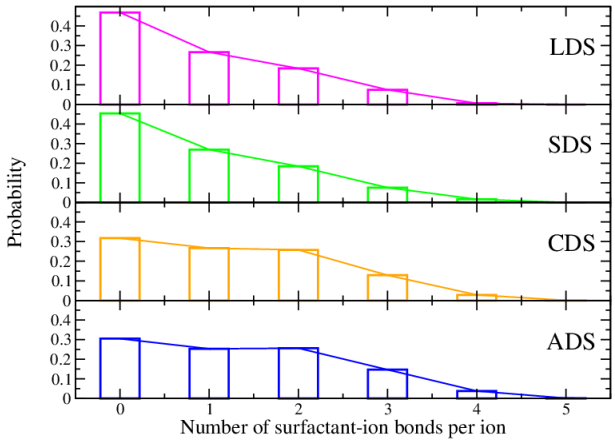

Fig. 9 Histograms showing the probability of an ion being bound to a given number of different DS^- headgroups.

ity measurements of micellar solutions of similar systems, with the one exception in which the value for LDS in our systems is slightly smaller than the experimental value (0.63 ± 0.07) [36]. Meanwhile, our values do not agree as well with the electrical conductivity measurements by Benrraou *et al.*, [39] but they do follow the same trend observed within their measurements $(\alpha(\text{CDS}) < \alpha(\text{SDS}))$.

Salt-bridging was investigated by constructing histograms of the probability of each different counterion species being bound to n surfactant headgroups through the duration of the production simulation runs, see Figure 9. For LDS and SDS, the probability of an ion interacting with n surfactants is monotonically decreasing with n. The corresponding histograms for CDS and ADS are distinctly different. First, a larger majority of the counterions in these systems are bound to at least one surfactant which is clear from the sharp decrease in $n = 0$ compared to the corresponding histograms for LDS and SDS. The probability of the Li^+, Na^+, Cs^+ and NH_4^+ ions being bound to at least one surfactant headgroup is 0.53, 0.55, 0.68 and 0.70 respectively. Second, there is an almost equal probability of a Cs^+ or NH_4^+ ion being bound to one or two surfactants. In fact, in the case of ADS, it is more probable for an ion to be interacting with two surfactant molecules than one. Additionally, ADS and CDS are approximately twice as likely to be bound to 3 surfactant headgroups as either LDS or SDS. There is also a non-negligible proportion of ions which are bound to 4 surfactant headgroups in all simulations. LDS has the smallest probability of this at 0.006, followed by SDS (0.02), CDS (0.03) and ADS (0.04). This indicates that salt-bridging is more prominent in the CDS and ADS systems than in LDS and SDS, which was also observed in the simulation study of LDS, SDS and ADS micelles carried out by Rakitin and Pack [40]. While we have kept the area per surfactant molecule constant in each of our simulated systems, this trend is consistent with the various studies that have found that the area per surfactant of ADS and CDS systems is smaller than those found for SDS and LDS systems [9,10].

It has been established that all of the different counterion species exhibit salt bridging with ions bound to different numbers of surfactant headgroups with ranging probabilities. To see how this process changes for varying numbers of bound headgroups, if at all, we calculated the distributions of Δz: the difference in the z-components of the position vectors of the counterion and S_{DS} atoms. We also calculated the S_{DS}-ION-S_{DS} angles. These distributions are shown in Figure 10.

For all simulations, there is a slight tendency for the Δz distributions to shift towards smaller values as the number of bound headgroups increases. This implies that for bridging events involving larger numbers of surfactant headgroups, the ion involved in the event is more likely to be situated level with the headgroups, with respect to the z direction, as opposed to being located towards the hydro-carbon tail region away from the bulk water. The S_{DS}-ION-S_{DS} angle distributions are directly related to Δz and thus it follows that the observed shift in Δz towards smaller values results in a shift of the S_{DS}-ION-S_{DS} angles towards smaller angles also. We would like to emphasize that this is a very slight affect.

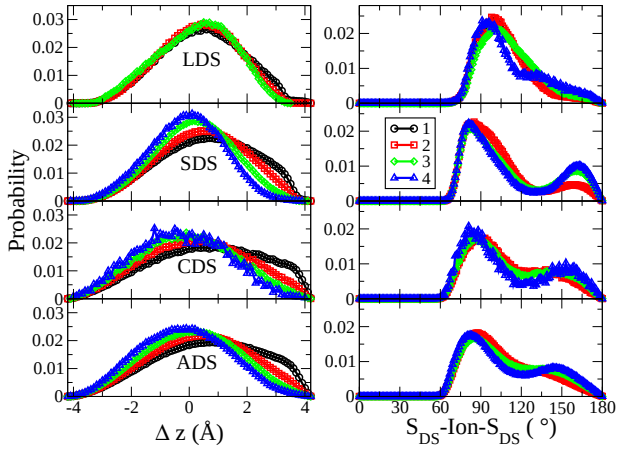

Fig. 10 Left: Probability distributions for Δz between sulfur atoms in DS^- and the counterions. Right: Probability distributions of the S_{DS}-ION-S_{DS} angles. The colours black, red, green and blue are used to represent distributions obtained from salt bridging events involving 1,2,3 and 4 DS^- headgroups, respectively.

Figure 11 shows an example of an ammonium ion from the ADS simulation involved in a bridging event between three surfactant headgroups. The snapshot provides visual evidence that the NH_4^+ ions form hydrogen bonds with the O_{DS} atoms in the DS^- headgroup, which was also suggested by the SDMs we have calculated.

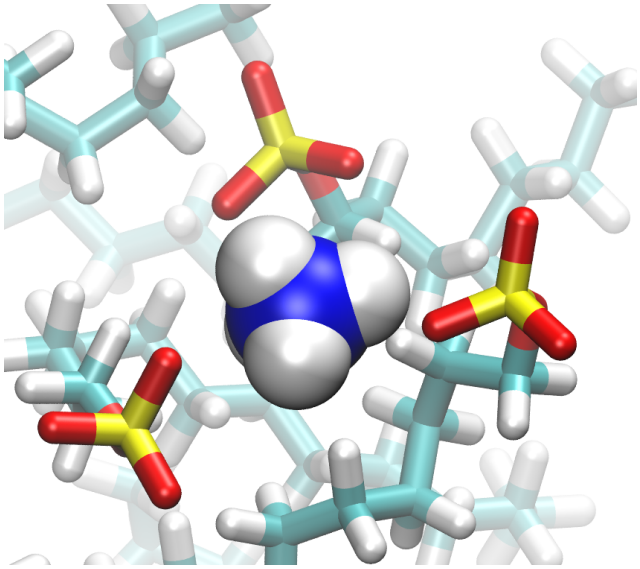

Fig. 11 Snapshot from the ADS simulation of a NH_4^+ ion bound to three different DS^- headgroups at one time. The colours cyan, grey, red, yellow and blue are used to represent the elements: carbon, hydrogen, oxygen, sulphur and nitrogen, respectively.

5 Conclusions

We have conducted all-atom molecular dynamics simulations of DS^- surfactant monolayers at the air/water interface with four different monovalent counterion species (Li^+, Na^+, Cs^+, NH_4^+) in order to determine how the structural and interfacial properties of the monolayers were affected.

In general, we observe very little effect of varying the counterion on the structure of the DS^- monolayers. However, we have observed significant differences in the interfacial properties of the monolayers in the presence of the different counterions. When taking all of the results compiled in this manuscript, the trend of the hydration of the DS^- headgroups in the presence of the various counterions can be explained via the following underlying mechanisms. In the ADS monolayers, the NH_4^+ ions directly compete with the hydrating water molecules for hydrogen bonds with the headgroup and in doing so cause these monolayers to be the least hydrated. In the case of the CDS system, the Cs^+ ions are strongly bound to the headgroup and are weakly hydrated, such that they would prefer to displace water in the DS^- hydration shell to interact with the headgroup. In the case of the Li^+ ions, they interact almost as strongly with the DS^- headgroups as the Na^+ ions, but are generally less hydrated than the Na^+ ions and therefore they bring less water to the monolayer interface than the Na^+ ions. There is a 1 water molecule difference in both the number of hydrating waters per cation and per DS^- headgroup in the two systems, so this seems to be the difference.

The differences in the interfaces that result from using the different counterions with the DS^- surfactants undoubtedly have significant implications on their ability to encapsulate solutes. One example of this is, as was mentioned in the Introduction, the results of some recent experimental work which show that ADS micelles have a poorer solubilisation capacity for encapsulating testosterone derivatives than SDS micelles, despite the fact that the ADS micelles have a larger aggregation number and lower hydration[35]. Taking into account the results presented in this manuscript, this could be due to strong interactions between the surfactant headgroups and the ammonium counterions. These interactions are strong enough to displace water molecules from the interface because of the ability of ammonium ions to form hydrogen bonds with the surfactant headgroups. Additionally, we see that there is a significant increase in the salt bridging between the DS^- headgroups when NH_4^+ ions are present than when Na^+ ions are, which would result in a stronger association between the headgroups at the micelle's surface.

The chemical structure of the poorly soluble molecule also plays a role in the ability to be solubilised within certain surfactant aggregates. For example, Kim *et al.* found that the solubilisation of pyrene in DS^- aggregates increases with increased aggregation numbers as the counterion is changed from Li^+ to Na^+ to NH_4^+ but the number of pyrene solubilised per surfactant molecule is only slightly increased[36]. Therefore, in the future, we will conduct further simulations to study the free energy landscape that results from the penetration of a variety of testosterone derivatives and other drugs into monolayers and micelles of the DS^- surfactants with different counterions. The results of these simulations will allow us to determine the free energy barriers that are required to be overcome in order to successfully encapsulate these drugs in these structures, and also understand the molecular mechanisms that are necessary to overcome them. In doing so, we aim to build on our previous work[59] on these systems to continue to develop an understanding of what role the underlying chemistry of the drug molecules and the surfactant molecules play in the encapsulation process.

6 Acknowledgements

The authors thank Dr. Jemma Trick and Dr. Richard J. Gillams for their help in proof reading and preparing the final presentation of this manuscript. D. T. A. and C. D. L. thank the EPSRC for the GTA studentship which funds D. T. A.'s research. Y. S. and M. J. L. thank the GETFund (Ghana Education Trust Fund) for funding the Ph.D. studentship of Y. S. Additionally, D. T. A. and C. D. L. acknowledge the stimulating research environment provided by the EPSRC Centre for Doctoral Training in Cross-Disciplinary Approaches to Non-Equilibrium Systems (CANES, EP/L015854/1). L. C. P. would like to acknowledge support from the Spanish MINECO (grants No. FIS2014-54734-P and FIS2012-39443-C02-01) and from the Government of Catalonia (grants No. 2009SGR-1003 and 2014SGR-00581). Finally, it is through our membership within the UK HPC Materials Chemistry Consortium, which is funded by the Office of Science and Technology through the EPSRC High End Computing Programme (Grant No. EP/L000202), that we were able to use the facilities of ARCHER, the UK National

Supercomputing Service (http://www.archer.ac.uk), to carry out aspects of this work.

References

1 L. I. Schramm, *Emulsions, Foams and Suspensions: Fundamentals and Applications*, WILEY-VCH Verag GmbH & Co. KGaA, 2005.

2 S. Paria and K. C. Khilar, *Adv. Drug Delivery Rev.*, 2000.

3 M. J. Lawrence and G. D. Rees, *Adv. Colloid Interface Sci.*, 2004.

4 B. E. Rabinow, *Nat. Rev. Drug Discovery*, 2004.

5 B. B. T. S. Mishra, B.; Patel, *Nanomed. Nanotechnol. Bio. Med.*, 2010.

6 L. Cohen, M. Martin, F. Soto, F. Trujillo and E. Sanchez, *J. Surfactants Deterg.*, 2016, **19**, 219–222.

7 T. S. Banipal, H. Kaur, A. Kaur and P. K. Banipal, *Food chemistry*, 2016, **190**, 599–606.

8 S. Kumar and A. Mandal, *Appl. Surf. Sci.*, 2016, **372**, 42–51.

9 J. R. Lu, A. Marrocco, T. J. Su, R. K. Thomas and J. Penfold, *J. Colloid Interface Sci.*, 1993, **158**, 303–316.

10 S. G. Oh and D. O. Shah, *J. Phys. Chem.*, 1993, **97**, 284–286.

11 J. R. Lu, M. Hromadova, E. A. Simister, R. K. Thomas and J. Penfold, *J. Phys. Chem.*, 1994, **98**, 11519–11526.

12 D. J. Lyttle, J. R. Lu, T. J. Su, R. K. Thomas and J. Penfold, *Langmuir*, 1995, **11**, 1001–1008.

13 J. Lu, R. Thomas and J. Penfold, *Adv. Colloid Interface Sci.*, 2000, **84**, 143–304.

14 T. Gilányi, I. Varga and R. Mészáros, *PCCP*, 2004, **6**, 4338–4346.

15 C. M. Johnson and E. Tyrode, *PCCP*, 2005, **7**, 2635–40.

16 V. L. Shapovalov and G. Brezesinski, *J. Phys. Chem. B*, 2006, **110**, 10032–40.

17 M. Sovago, G. W. H. Wurpel, M. Smits, M. Müller and M. Bonn, *J. Am. Chem. Soc.*, 2007, **129**, 11079–84.

18 C. Wang and H. Morgner, *Langmuir*, 2010, **26**, 3121–5.

19 P. Brown, C. Butts, R. Dyer, J. Eastoe, I. Grillo, F. Guittard, S. Rogers and R. Heenan, *Langmuir*, 2011, **27**, 4563–71.

20 R. A. Livingstone, Y. Nagata, M. Bonn and E. H. G. Backus, *J. Am. Chem. Soc.*, 2015, **137**, 14912–9.

21 A. P. Dabkowska, L. E. Collins, D. J. Barlow, R. Barker, S. E. McLain, M. J. Lawrence and C. D. Lorenz, *J. Chem. Phys.*, 2016, **144**, 225101.

22 D. Hu, A. Mafi and K. C. Chou, *J. Phys. Chem. B*, 2016.

23 K. J. Schweighofer, U. Essmann and M. Berkowitz, *J. Phys. Chem. B*, 1997, **101**, 3793–3799.

24 P. A. Kralchevsky, K. D. Danov, G. Broze and A. Mehreteab, *Langmuir*, 1999, **15**, 2351–2365.

25 H. Kuhn and H. Rehage, *J. Phys. Chem. B*, 1999, **103**, 8493–8501.

26 H. Dominguez and M. L. Berkowitz, *J. Phys. Chem. B*, 2000, **104**, 5302–5308.

27 C. D. Lorenz and A. Travesset, *Langmuir*, 2006, **22**, 10016–10024.

28 G. Hantal, L. B. Partay, I. Varga, P. Jedlovszky and T. Gilányi, *J. Phys. Chem. B*, 2007, **111**, 1769–74.

29 J. J. Giner Casares, L. Camacho, M. T. Martín-Romero and J. J. López Cascales, *ChemPhysChem*, 2008, **9**, 2538–43.

30 L. Shi, N. R. Tummala and A. Striolo, *Langmuir*, 2010, **26**, 5462–74.

31 T. Zhao, G. Xu, S. Yuan, Y. Chen and H. Yan, *J. Phys. Chem. B*, 2010, **114**, 5025–33.

32 H. Yan, X.-L. Guo, S.-L. Yuan and C.-B. Liu, *Langmuir*, 2011, **27**, 5762–71.

33 M. Chen, X. Lu, X. Liu, Q. Hou, Y. Zhu and H. Zhou, *Langmuir*, 2014, **30**, 10600–7.

34 M. Chen, X. Lu, X. Liu, Q. Hou, Y. Zhu and H. Zhou, *J. Phys. Chem. C*, 2014, **118**, 19205–19213.

35 Y. Saaka, *Ph.D. Thesis*, University of London, 2016.

36 J.-H. Kim, M. M. Domach and R. D. Tilton, *Langmuir*, 2000, **16**, 10037–10043.

37 S. S. Berr, M. J. Coleman, R. R. M. Jones and J. S. Johnson, *J. Phys. Chem.*, 1986, **90**, 6492–6499.

38 S. Chen, *Ann. Rev. Phy. Chem.*, 1986, **37**, 351–399.

39 M. Benrraou, B. L. Bales and R. Zana, *J. Phys. Chem. B*, 2003, **107**, 13432–13440.

40 A. R. Rakitin and G. R. Pack, *J. Phys. Chem. B*, 2004, **108**, 2712–2716.

41 C. M. Tcacenco, R. Zana and B. L. Bales, *J. Phys. Chem. B*, 2005, **109**, 15997–6004.

42 M. Sammalkorpi, M. Karttunen and M. Haataja, *J. Phys. Chem. B*, 2009, **113**, 5863–70.

43 N. Schwierz, D. Horinek, U. Sivan and R. R. Netz, *Curr. Opin. Colloid. In.*, 2016.

44 D. Bastos-González, L. Pérez-Fuentes, C. Drummond and J. Faraudo, *Curr. Opin. Colloid. In.*, 2016, **23**, 19–28.

45 U. Sivan, *Curr. Opin. Colloid. In.*, 2016.

46 F. Hofmeister, *Archiv für experimentelle Pathologie und Pharmakologie*, 1888, **25**, 1–30.

47 W. Kunz, J. Henle and B. Ninham, *Curr. Opin. Colloid. In.*, 2004, **9**, 19–37.

48 W. Kunz, *Specific Ion Effects*, Wiley & Sons, 2007.

49 T. Kawai, H. Kamio, T. Kondo and K. Kon-No, *J. Phys. Chem. B*, 2005, **109**, 4497–500.

50 L. Martinez, R. Andrade, E. G. Birgin and J. M. Martinez, *J. Comput. Chem.*, 2009, **30**, 2157–64.

51 S. Plimpton, *J. Comput. Phys.*, 1995, **117**, 1 – 19.

52 K. Vanommeslaeghe, E. Hatcher, C. Acharya, S. Kundu, S. Zhong, J. Shim, E. Darian, O. Guvench, P. Lopes, I. Vorobyov and A. D. J. MacKerell, *J. Comput. Chem.*, 2010, **31**, 671–690.

53 W. Yu, K. Vanommeslaeghe and A. D. J. MacKerell, *J. Comput. Chem.*, 2012, **33**, 2451–2468.

54 J. B. Klauda, R. M. Venable, J. A. Freites, J. W. O' Connor, D. J. Tobias, C. Mondragon-Ramirez, I. Vorobyov, A. D. J. MacKerell and R. W. Pastor, *J. Phys. Chem. B, volume=114, pages=7830-7843, year=2010,*.

55 R. W. Pastor and A. D. J. MacKerell, *J. Phys. Chem. Lett.*, 2011, **2**, 1526–1532.
56 W. L. Jorgensen, J. Chandrasekhar, J. D. Madura, R. W. Impey and M. L. Klein, *J. Chem. Phys.*, 1983, **79**, 926–935.
57 W. I. Reiher, *Theoretical Studies of Hydrogen Bonding*, Ph.D. dissertation, Harvard University, 1985.
58 X. Tang, P. H. Koenig and R. G. Larson, *J. Phys. Chem. B*, 2014, **118**, 3864–3880.
59 D. T. Allen, Y. Saaka, M. J. Lawrence and C. D. Lorenz, *J. Phys. Chem. B*, 2014, **118**, 13192–201.
60 T. Darden, D. York and L. Pedersen, *J. Chem. Phys.*, 1993, **98**, 10089–10092.
61 W. G. Hoover, *Phys. Rev. A*, 1985, **31**, 1695–1697.
62 J.-P. Ryckaert, G. Ciccotti and H. J. Berendsen, *J. Comput. Phys.*, 1977, **23**, 327 – 341.
63 E. Chacón and P. Tarazona, *Phys. Rev. Lett.*, 2003, **91**, 166103.
64 H. Martínez, E. Chacón, P. Tarazona and F. Bresme, *P. Roy. Soc. Lond. A Mat.*, 2011, **467**, 1939–1958.
65 A. P. Willard and D. Chandler, *J. Phys. Chem. B*, 2010, **114**, 1954–1958.
66 S. A. Pandit, D. Bostick and M. L. Berkowitz, *J. Chem. Phys.*, 2003, **119**, 2199–2205.
67 M. L. San-Román, M. Carrillo-Tripp, H. Saint-Martin, J. Hernández-Cobos and I. Ortega-Blake, *Theor. Chem. Acc.*, 2006, **115**, 177–189.
68 C. N. Rowley and B. Roux, *J. Chem. Theory Comput.*, 2012, **8**, 3526–3535.
69 C. F. Schwenk, T. S. Hofer, and B. M. Rode*, *J. Phys. Chem. A*, 2004, **108**, 1509–1514.
70 W. L. Jorgensen and J. Gao, *J. Phys. Chem.*, 1986, **90**, 2174–2182.